JOURNAL INDIAN ASSOCIATION OF SEDIMENTOLOGISTS ISSN NO 2582 – 2020
Vol. 43, Issue I, 2026, pp 37 – 52

A comparative study on the petrography, provenance and tectonic settings with evolution patterns with the Neogene Lithosequence in the Siwalik Belt, Arunachal Pradesh and the Belt of Schuppen, Naga-Patkai Hills, India

Abhijit Chakraborty[1*], Monmohan Gogoi[1], Persona Gogoi[1], Ranjan Kumar Sarmah[1], Diganta Bhuyan[1]
[1]K.D.M. Chair, Department of Applied Geology, Dibrugarh University, Dibrugarh, 786004, India

ARTICLE INFO

KEYWORDS:

Neogene rock formations;

Siwalik fold-thrust belt;

Belt of Schuppen;

Himalayan orogens;

Rock fragments;

Recycled orogenic;

ABSTRACT

This study presents a comparative analysis of Neogene sandstones from two tectonically active regions in Northeast India-the Siwalik Belt of Arunachal Pradesh and the Belt of Schuppen in the Naga-Patkai Hills. Petrographic examination of 40 thin sections (20 from each region) was conducted to assess mineralogical composition, provenance, and tectonic implications. Quartz is the dominant framework grain, ranging between 48% and 56.6%. Variations in quartz texture, particularly the proportion of undulatory monocrystalline and polycrystalline types, reflect differing degrees of tectonic compaction and sediment recycling. Mica content, especially the presence of kink-banded muscovite, further indicates deformation intensity during burial.

In the Schuppen Belt, Tipam Sandstones at Tipong-Pani contain more sedimentary fragments, while Namchik-Namphuk samples are richer in metamorphic and igneous clasts, consistent with rapid uplift of the Mishmi Hills. In contrast, the Siwalik Belt samples from Kimin-Ziro and Likabali-Garo show higher proportions of undulatory quartz and metamorphic fragments, pointing to a recycled orogenic source from the Higher and Lesser Himalayas. Feldspar textures and matrix content suggest variable depositional energy across the formations.

Provenance plots (QFL and QmFLt) confirm a quartzose recycled origin for both belts. These mineralogical signatures, particularly the deformation textures in quartz and mica, offer insights into the tectono-sedimentary evolution of the Himalayan foreland and associated orogenic systems during the Neogene.

INTRODUCTION

The Northeastern margin of the Indian subcontinent represents a tectonically active and structurally complex zone, defined by the convergence of the Indian, Eurasian, and Burma plates. This interaction has resulted in prominent foreland basin development and deformation features, particularly expressed in the Siwalik Belt of Arunachal Pradesh and the Belt of Schuppen in the Naga-Patkai Hills. These belts preserve significant records of Neogene sedimentation associated with the uplift of the Himalayas and the Indo-Burman Ranges.

Previous studies have extensively described the fluvial-deltaic nature of the Siwalik sediments (Bezbaruah and Goswami, 2013) and the tectonic imbrication in the Schuppen Belt that hosts the Tipam and Barail Groups' formations (Borgohain et al., 2023). However, existing literature has focused more on structural or lithostratigraphic aspects, often overlooking the comparative sedimentological signatures, provenance variations, and mineralogical maturity between these two belts. Furthermore, a region-specific synthesis that integrates modal mineralogy with tectonic evolution, especially focusing on quartz and mica variability, remains insufficiently addressed. So, the present study is an attempt to address the problems related to the tectono-sedimentation history of these two belts, i.e., the Siwalik belt and the Belt of Schuppen.

This integrated approach offers insights into how active tectonics and foreland basin evolution have jointly influenced sedimentation patterns in northeastern India during the Miocene-Pliocene interval.

GEOLOGY OF THE STUDY AREA

The Belt of Schuppen, extending from Haflong in the southwest to Manabhum in the northeast, forms a narrow, linear zone characterized by a series of overthrusts arranged in an imbricate pattern. The region is primarily composed of Tertiary rocks, with the Neogene formations representing the dominant lithological units. This belt encompasses key coal-bearing areas such as Makum, Dilli-Joypur, Tipong-Pani, and Namchik-Namphuk, where well-exposed successions of the Barail and Tipam Groups are observed (Sarma and Chutia, 2013). The Tipam Sandstone, a principal unit within this group, is typically light grey,

*Corresponding Author
Email: abhijitgeology2021@gmail.com
DOI: https://doi.org/10.51710/jias.v43iI.400
Received 12 December 2024; Received in revised form 16 October 2025; Accepted 15 April 2026
Available online 30 June 2026

fine- to medium-grained, and moderately hard, often interbedded with clay layers that exhibit mottled coloration and become plastic when wet. These lithologies are prominently exposed along the Tipong-Pani and Namchik-Namphuk sections (Fig. 1).

In contrast, the Siwalik fold-thrust belt in Arunachal Pradesh extends from the Himalayan Frontal Thrust (HFT) to the Main Boundary Thrust (MBT) and

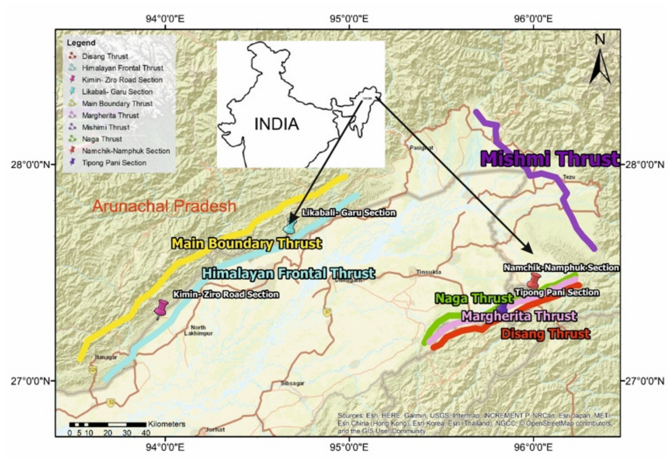

Fig. 1. Location Map of the Study Areas

displays a well-defined lithostratigraphy. This belt comprises a tripartite division of Neogene formations-Dafla, Subansiri, and Kimin-corresponding to the Lower, Middle, and Upper Siwaliks, respectively. These formations were deposited predominantly in fluvial to deltaic settings and are exposed along the Kimin-Ziro and Likabali-Garo Road sections. The Dafla Formation is typically conglomeratic and coarse-grained, transitioning upward into the finer-grained Subansiri and Kimin Formations. These sequences collectively record a history of active sedimentation linked to the progressive uplift of the Himalayas and foreland basin development (Catlos et al., 2004).

A comparative lithostratigraphic framework of these two belts is presented in Tables 1 and 2, highlighting key differences in lithology and depositional architecture. The spatial distribution of study sections is illustrated in Fig. 1, which delineates the structural configuration of the study area. (Sarma and Chutia, 2013).

MATERIALS AND METHODS

A total of 40 representative sandstone samples were systematically collected from two major tectonically active regions in Northeast India: 20 samples from the Belt of Schuppen (Namchik-Namphuk and Tipong-Pani sections) and 20 from the Siwalik Belt (Kimin-Ziro and Likabali-Garo sections). Sample selection was guided by lithological variability, stratigraphic position, and accessibility of well-exposed outcrops.

Each sample was processed for thin-section preparation following standard petrographic procedures. Modal analysis was conducted using a Leica DM750P polarizing microscope, adhering to the point-counting method described by Carver (1971). For each thin section, a minimum of 300 framework grains were counted to obtain statistically robust mineral proportions, including quartz (monocrystalline undulatory, non-undulatory, and polycrystalline types), feldspar, mica, and lithic fragments. Comparative petrographic analysis focused on grain type, textural maturity, and diagenetic features. Special attention was given to the identification of deformation textures in

Table 1: Lithostratigraphic Succession of the Study Area of Naga Schuppen Belt (Borgohain et al., 2023).

Age	Group	Formation	Lithology
Pleistocene to Recent		Terrace deposit	Boulder beds
-------------------------------------Unconformity-------------------------------------			
Mio-Pliocene	Tipam Group	Girujan Clay Formation	Mottled clay with intervening sandstone
Miocene		Tipam Sandstone Formation	Alternating beds of sandstone and shales with subordinate clays

mica (e.g., kink banding) and quartz (e.g., undulatory extinction), which serve as indicators of tectonic stress and burial compaction. To interpret sediment provenance and tectonic setting, compositional data were plotted on established ternary diagrams: QFL (quartz-feldspar-lithics) and QmFLt (monocrystalline quartz-feldspar-total lithics), following Dickinson (1985), and provenance classification diagrams after Basu et al. (1975) and Tortosa et al. (1991). These diagrams enabled the differentiation between recycled orogenic, metamorphic, and plutonic sources. In addition, recalculated values of quartz (Q), feldspar (F), and lithic fragments (L) were normalized to 100% to facilitate inter-sample comparison. Rock fragment counts were further subdivided into sedimentary, metamorphic, and igneous types, and recalculated as percentages of total lithics for provenance determination (Krumbein and Pettijohn, 1938) and (Boggs, 2013). All data were interpreted comparatively between the two belts to evaluate the influence of differing tectonic regimes on sedimentary maturity, provenance, and depositional processes across the Brahmaputra arc.

RESULTS

Sandstone Petrography

Thin-section petrography of the Tipam Sandstone reveals that quartz is the dominant framework grain in both Namchik-Namphuk and Tipong-Pani sections Quartz content reaches up to 56.58% in Tipong-Pani, predominantly monocrystalline and non-undulatory in texture (39.27%), indicating relatively stable conditions during transport (Fig. 2M). Namchik-Namphuk samples, in contrast, show a higher proportion of monocrystalline

Table 2: Lithostratigraphic Succession of the Study area of Siwalik Belt (GSI, 2010; Kumar, 1997)

Age	Group	Formation	Lithology
-------------------------------- Main Frontal Fault--			
Mio-Pliocene	Siwalik Group	Kimin (Upper Siwalik)	Alternations of soft, grey sandstone, silt, clay and gravelly boulder beds Carbonised wood and plant fossils. Gradational contact
Mio-Pliocene		Subansiri (Middle Siwalik)	Sandstone, grey micaceous and salt and pepper texture and calcareous concretions. Clay and claystone in the upper part. Vertebrate fossil Bos sp.
Miocene		Dafla (Lower Siwalik)	Sandstone, hard, grayish white to greenish grey, khaki grey shale alternations. Plant fossils

Fig. 2. Sandstone petrography; A: Corrosion of quartz grains by argillaceous matrix, B: Development of Muscovite from argillaceous matrix, C: Non-undulatory quartz with clay altered cements, D: Polycrystalline quartz >3 units, E: Mica kinking, F: Igneous rock fragment, G: Zircon, H: Microcline, I: Development of two mica grains, J: Fine grained sandstone, K: Polycrystalline Quartz, L: Matrix, M: Non undulatory quartz, N: Undulatory quartz, O: Metamorphic rock fragment, P: Sedimentary Rock Fragment undulatory quartz (Fig. 2N), indicative of a low-grade metamorphic origin. Polycrystalline quartz, often composed of more than three sub-units, is also observed (Fig. 2D, K), pointing to a metamorphic source. Feldspars, including plagioclase with lamellar twinning and microcline showing cross-hatched twinning (Fig. 2H), and mica with kink bands (Fig. 2E, I), are common. The presence of argillaceous matrix and ferruginous cement varies among samples (Fig. 2A, B, C, J, L). Lithic fragments include sedimentary (Fig. 2P), igneous (Fig. 2F), and metamorphic clasts (Fig. 2O), (Table 3).

Quartz content in these sections ranges from 48-55%, with monocrystalline undulatory quartz being dominant, especially in the Likabali-Garo section (Fig. 3A and L). Polycrystalline quartz and fractured grains are also observed (Fig. 3E, F, and K), accompanied by 6-8% metamorphic lithic fragments (Fig. 3Q). Feldspar types include microcline and plagioclase, both with deformation features such as overgrowth and twinning (Fig. 3J, P, R). Mica is present in both kinked and overgrown forms (Fig. 3H, I, M, and N). High matrix content is noted in parts of the Likabali-Garo section (Fig. 3B, C, D, O), indicating lower depositional energy. (Table 4). These findings are based on petrographic analyses of sandstone thin sections of all four areas that samples are collected, highlighting features like distribution of different types of rock-fragments, quartz, mica, feldspar, matrix and cement types, indicative of their diverse origins and evolution of the Naga Schuppen belt and Siwalik Belt (Grantham et al., 1988) (Table 5).

PROVENANCE AND TECTONIC SETTING

Quartz Type Distribution and Framework Composition

Modal petrographic analysis of Neogene sandstones from the Namchik–Namphuk, Tipong–Pani, Likabali–Garo, and Kimin–Ziro sections demonstrates a regionally coherent quartzose framework composition with diagnostic variations that directly reflect progressive unroofing of an active orogenic hinterland. Quartz overwhelmingly dominates the framework fraction in all four sections, confirming compositional maturity and substantial sediment recycling. However, systematic differences in quartz types provide critical tectonic signals.

Monocrystalline undulatory quartz is particularly abundant in the Namchik–Namphuk and Likabali–Garo sections, indicating substantial derivation from metamorphic terranes subjected to tectonic strain. In contrast, the increased proportion of monocrystalline non-undulatory quartz in parts

Table 3: Result of Model analysis of Namchik- Namphuk and Tipong- Pani Section

Sl. No.	Sample no	Q_{mu}	Q_{mn}	Q_p (2-3 unit)	Q_p (>3 unit)	Q_{total}	Feldspar	Rock fragment				Mica	Matrix	cement	Chert
								Ig	Sed	Meta	Total				
1	NR1	39.4	12.1	3.71	1.2	56.4	6.84	3.52	1.49	5.64	10.65	2.5	12.05	9.5	2
2	NR2	33.3	11.2	2.6	2.1	49.2	42.2	3.16	2.07	4.97	10.2	3.5	19.47	10.7	2.71
3	NR3	20.6	23.09	1.08	0	44.8	8.87	2.53	0.81	2.78	6.22	5.5	23.5	12.2	0.78
4	NR4	6.86	25.77	0	5.91	38.54	9.46	2.871	11.89	7.469	22.23	2.6	12.05	9.93	5.19
5	NR5	5.47	34.73	1.23	8.87	50.3	6.53	0.924	1.91	8.006	10.84	6.45	13.55	10.1	2.23
6	NR6	31.7	8.48	2.74	2.98	45.88	2.25	1.003	6.73	0.664	7.73	6.84	19.21	17.09	1
7	NR7	33.2	7.2	11.08	12.65	64.13	2.85	0.86	1.29	6.63	8.86	2.84	14.55	5.75	1.03
8	NR8	14.3	29.66	5	5.6	54.56	5	2.97	4.06	9.54	15.66	3	14	5.45	1.33
9	NR9	30.2	18.3	4	1.9	54.4	4.5	2.096	1.004	8.4	11.5	5	13.3	8.8	2
Results of modal analysis of Tipam Sandstone Formation of Namchik river section															
10	4(C)	3.69	45.60	1.38	0.77	51.44	1.99	3.14	1.82	7.12	11.08	3.08	19.5	12.7	3.22
11	2(I)	5.56	44.24	1.32	0.84	51.96	1.59	1.28	13.44	5.06	19.32	1.22	14.5	11.3	3.20
12	2(D)	2.17	51.29	0.31	0.20	53.97	0.51	1.975	9.43	3.98	15.63	0.72	20.31	8.80	4.12
13	2(H)	4.07	40.73	1.12	0.20	46.82	2.23	1.62	13.065	3.05	17.4	3.36	15.47	15.37	4.42
14	P (3)	50.25	24.7	0.28	0.64	75.87	4.28	0.53	6.1	1.43	7.53	0.6	14.35	1.86	1.62
15	P (4)	2.62	50.36	1.6	0.72	55.3	0.29	4.04	10.05	2.65	14.74	2.0	15.91	11.5	2.25
16	P (5)	28.93	18.0	1.60	12.21	60.74	11.57	4.002	14.6	1.9	19.5	4.18	2.89	0.66	2.37
17	P (6)	18.31	13.56	9.44	11.775	53.085	7.58	2.5	4.425	2.091	8.94	4.25	13.55	8.535	4.06
18	P (7)	17.91	13.16	9.23	10.775	51.075	3.245	1.097	8.438	2.005	11.54	2.85	15.94	9.84	5.51
19	P (8)	18.34	13.09	9.63	11.15	52.65	5.59	0.095	6.9	3.95	11.94	4.25	17.02	3.83	5.72
20	P (9)	16.71	8.03	11.96	18.29	54.99	5.98	1.66	6.47	2.21	10.34	2.65	12.17	10.32	5.13
Result of Model analysis of Tipam sandstone Formation of Tipong-Pani river section															


A
200 µm
B
500 µm
C
500 µm
D
200 µm
E
500 µm
F
200 µm
G
200 µm
H
200 µm
I
500 µm
J
200 µm
K
500 µm
L
500 µm
M
200 µm
N
200 µm
O
500 µm

Fig. 3. A: Weathered and Fractured Quartz, B: Argillaceous and ferruginous cement occupying intergranular spaces, C: Chert, D: siliceous and argillaceous Cement, E: Fractured Quartz, F: Polycrystalline Quartz, G: Mica kinking, H: Microcline, I: Inclusion Muscovite, J: Feldspar, K: Polycrystalline Quartz, L: Monocrystalline Quartz, M: Muscovite, N: Overgrowth of Muscovite, O: Argillaceous and ferruginous cement occupying intergranular spaces, P: Overgrowth of Microcline, Q: Metamorphic rock fragments, and R: Microcline

of the Tipong–Pani section and within the Kimin Formation of the Kimin–Ziro section reflects enhanced contribution from plutonic sources exposed during deeper levels of exhumation. The widespread presence of polycrystalline quartz across all sections further substantiates derivation from low- to high-grade metamorphic complexes.

Framework classification following Folk (1980) shows that most samples fall within the Sublitharenite and Feldspathic Litharenite fields, with localized Litharenite compositions where lithic fragments increase (Fig. 4). Metamorphic lithic fragments dominate in the Likabali–Garo and Kimin–Ziro sections, whereas sedimentary lithics and argillaceous matrix are relatively more abundant in the Tipong–Pani section. Overall matrix content remains low to moderate, indicating moderate compositional maturity and effective sediment winnowing. Collectively, these petrographic characteristics demonstrate erosion of a heterogeneous orogenic belt exposing metamorphic basement rocks and granitoid intrusions, with sedimentary recycling superimposed upon primary basement unroofing.

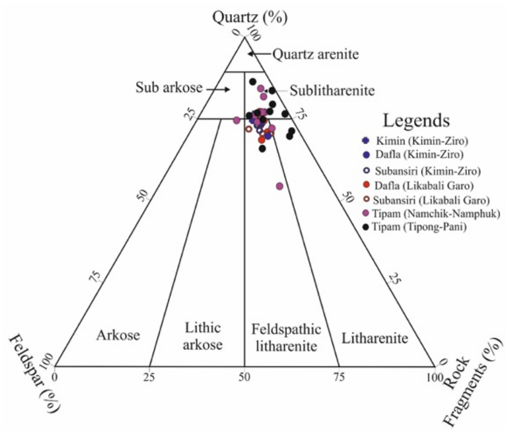

Fig. 4. QFR ternary diagram after Folk (1980) showing the modal composition and sandstone classification of samples from all four sections

Table 4: Result of Model analysis of Likabali- Garo and Kimin-Ziro Road Section															
Sl. No.	Sample no	Q_{mu}	Q_{mn}	Q_p (2-3 unit)	Q_p (>3 unit)	Q_{total}	Feldspar	Rock fragment				Mica	Matrix	cement	Chert
								Igneous	Sedimentary	Metamorphic	Total				
21	LG 4(2)	16.55	12.3	8.07	10.95	47.87	6.14	0.65	1.25	8.1	10	4.4	21.47	3.14	6.98
22	LG 9(3)	16.95	10.9	6.87	12.42	47.14	5.44	2.35	2	9.13	13.48	2.62	20.09	4.21	7.02
23	LG 10 (1)	17.95	11.5	8.47	11.01	48.93	7.74	1.07	1.13	12.08	14.28	3.92	19.21	3.98	1.94
24	LG 13	18.75	12.8	8.31	11.09	50.95	6.44	1.56	0.86	8.36	10.78	4.52	20.09	3.76	3.46
25	LG 19 (2)	16.05	14	6.27	14.72	51.04	5.04	1.01	3.87	7.21	12.09	2.02	19.93	3.97	5.91
26	LG 21 (3)	18.05	12.2	7.97	11.22	49.44	6.04	0.73	1.65	9.5	11.88	4.32	18.25	5.23	5.84
Result of Model analysis of Dafla Formation of Likabali-Garo section															
27	LG 23	16.76	10.93	12.4	13.68	53.77	5	1.2	1.77	7.4	10.37	2.31	14.07	9.49	4.99
28	LG 25	18.76	9.93	10.4	8.94	48.03	5.1	2.07	3.22	9.08	14.37	3.31	16.68	8.91	4.6
29	LG 31	17.21	8.41	10	12.46	48.08	8.48	2.22	1.8	5.82	9.84	6.15	14.84	7.86	4.75
30	LG 35	14.26	8.43	13.9	14.18	50.77	5.6	3.74	3.38	3.75	10.87	8.7	12.05	8.12	3.89
31	LG 39 (2)	17.31	12.56	8.63	10.46	48.96	6.58	2.305	2.385	6.25	10.94	5.25	12.65	9.39	6.23

32	LG 44	17.51	12.76	8.58	10.2	49.05	6.78	1.1	1.015	11.025	13.14	3.45	14.57	10.1	3.91
Result of Model analysis of Subansiri Formation of Likabali-Garo section															
33	KZ 1(2)	22.05	29.94	3.08	1.13	56.2	6.84	2.1	0.45	8.1	10.65	2.04	13.47	8.84	1.96
34	KZ 3	21.54	31.16	1.07	0.4	54.17	6.43	2.03	2.05	8.62	12.7	3.19	11.54	9.14	2.83
35	KZ 6	19.04	30.98	1.435	0.8	52.255	6.32	1.59	0.9	6.93	9.42	4.2	15.04	10.065	2.7
36	KZ 8	23.98	28.7	1.2	1.4	55.28	7.82	0.599	0.591	9.5	10.69	3.34	13.86	7.96	1.05
Result of Model analysis of Kimin Formation of Kimin-Ziro section															
37	KZ 12	17.45	11.7	7.27	11.02	47.44	5.94	4.1	3.09	6.89	14.08	3.02	18.92	5.18	5.42
38	KZ 14	14.8	8.17	10.41	15.98	49.36	6.02	1.33	1	8.55	10.88	3.14	19.74	4.93	5.93
Result of Model analysis of Dafla Formation of Kimin-Ziro section															
39	KZ 17	15.76	9.93	11.4	12.68	49.77	7.1	10.07	0.4	1.9	12.37	4.31	16.02	6.24	4.19
40	KZ 22	17.71	12.96	9.03	10.575	50.275	6.98	1.1	0.6	9.64	11.34	3.65	16.77	7.005	3.98
Result of Model analysis of Subansiri Formation of Kimin-Ziro section															

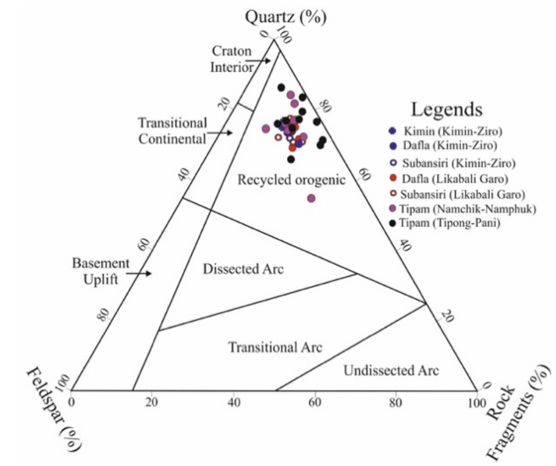

Fig. 5. QFL ternary diagram (Dickinson, 1985) showing the provenance fields of sandstones from all four sections.

Provenance Interpretation via Tectonic Discrimination Diagrams

Tectonic discrimination diagrams provide unequivocal evidence for a recycled orogenic provenance across the entire study area. On the QFL ternary diagram (Dickinson et al., 1983; Dickinson, 1985), samples from all four sections consistently cluster within the recycled orogen field (Fig. 5). This uniform distribution is not incidental; it reflects sediment supply from uplifted fold–thrust belts where previously deposited sedimentary successions and deformed basement rocks were actively eroded and recycled.

The QmFLt diagram reinforces this interpretation, with nearly all samples plotting

Table 5: Recalculated values of Q, F, L and Qm, F, L															
Sl. No.	Sample no	Actual % of Q, F and L				Recalculated % of Q, F and L			Actual % of Q_m, F and L				Recalculated % of Q_m, F and L		
		Q	F	L	Total	Q	F	L	Q_m	F	L	Total	Q_m	F	L
1	NR1	56.4	6.84	10.65	73.89	76.32	9.25	14.41	51.5	6.84	10.65	68.99	74.65	9.91	15.44
2	NR2	49.2	4.22	10.2	63.42	77.57	6.65	16.08	44.5	4.22	10.2	58.92	75.53	7.16	17.31
3	NR3	44.9	8.87	6.22	59.99	74.84	14.78	10.37	43.69	8.87	6.22	58.78	74.79	15.09	10.58
4	NR4	38.54	9.46	22.23	70.23	54.87	13.47	31.65	32.63	9.46	22.23	64.32	50.73	14.71	34.56
5	NR5	50.30	6.53	10.84	67.67	74.33	9.64	16.01	40.2	6.53	10.84	57.57	69.83	11.34	18.83
6	NR6	45.88	2.25	7.73	55.86	82.13	4.02	13.83	40.18	2.25	7.73	50.16	80.10	4.49	15.41
7	NR7	64.24	2.84	8.86	75.94	84.58	3.75	11.66	40.4	2.84	8.86	51.84	77.93	5.48	17.09
8	NR8	54.56	5	15.66	75.22	72.53	6.65	20.82	43.96	5	15.66	64.62	68.03	7.74	24.23
9	NR9	54.4	4.5	11.5	70.4	77.27	6.39	16.34	38.5	4.5	11.5	54.5	70.64	8.26	21.10
Recalculated values of Q, F, L and Q_m, F, L of the Tipam sandstones of Namchik river section															
10	4(C)	51.44	1.99	11.08	64.51	79.73	3.08	17.17	49.29	1.99	11.08	62.36	79.04	3.19	17.76
11	2(I)	51.96	1.59	19.32	72.87	71.30	2.18	26.15	49.8	1.59	19.32	70.71	70.42	2.24	27.32
12	2(D)	53.97	0.51	15.63	70.11	76.97	0.72	22.29	53.46	0.51	15.63	55.6	96.15	0.91	28.11
13	2(H)	46.12	2.23	17.4	63.82	70.14	3.39	26.46	44.80	2.23	17.4	64.43	69.53	3.46	27.0
14	P(3)	75.87	4.28	7.53	87.68	86.53	4.88	8.58	74.95	4.28	7.53	86.76	86.38	4.93	8.67
15	P(4)	55.3	0.29	14.74	70.33	78.6	0.29	14.74	52.98	0.29	14.74	68.01	77.90	0.42	21.67
16	P(5)	60.74	11.57	19.5	91.81	66.15	12.60	21.23	46.93	11.57	19.5	78	60.16	14.83	25

17	P(6)	53.085	7.58	8.94	69.605	76.266	10.89	12.844	31.87	7.58	8.94	48.39	65.861	15.664	18.475
18	P(7)	51.075	3.245	11.54	65.86	77.551	4.9271	17.522	31.07	3.245	11.54	45.855	67.757	7.0767	25.166
19	P(8)	52.65	5.59	11.94	70.18	75.021	7.9652	17.013	31.87	5.59	11.94	49.4	64.514	11.316	24.17
20	P(9)	54.99	5.98	10.34	71.31	77.114	8.3859	14.5	24.74	5.98	10.34	41.06	60.253	14.564	25.183
Recalculated values of Q, F, L and Q_m, F, L of the Tipam sandstones of Tipong-Pani river section															
21	LG 4(2)	47.87	6.14	10	64.01	74.785	9.5923	15.623	28.85	6.14	10	44.99	64.125	13.647	22.227
22	LG 9(3)	47.14	5.44	13.48	66.06	71.359	8.2349	20.406	27.85	5.44	13.48	46.77	59.547	11.631	28.822
23	LG 10 (1)	48.93	7.74	14.28	70.95	68.964	10.909	20.127	29.45	7.74	14.28	51.47	57.218	15.038	27.744
24	LG 13	50.95	6.44	10.78	68.17	74.74	9.447	15.813	31.55	6.44	10.78	48.77	64.691	13.205	22.104
25	LG 19 (2)	51.04	5.04	12.09	68.17	74.872	7.3933	17.735	30.05	5.04	12.09	47.18	63.692	10.682	25.625
26	LG 21 (3)	49.44	6.04	11.88	67.36	73.397	8.9667	17.637	30.25	6.04	11.88	48.17	62.798	12.539	24.663
Recalculated Value of Q, F, L and Q_m, F, L of Dafla Formation of Likabali-Garo section															
27	LG 23	53.77	5	10.37	69.14	77.77	7.2317	14.999	27.69	5	10.37	43.06	64.306	11.612	24.083
28	LG 25	48.03	5.1	14.37	67.5	71.156	7.5556	21.289	28.69	5.1	14.37	48.16	59.572	10.59	29.838
29	LG 31	48.08	8.48	9.84	66.4	72.41	12.771	14.819	25.62	8.48	9.84	43.94	58.307	19.299	22.394
30	LG 35	50.77	5.6	10.87	67.24	75.506	8.3284	16.166	22.69	5.6	10.87	39.16	57.942	14.3	27.758
31	LG 39 (2)	48.96	6.58	10.94	66.48	73.646	9.8977	16.456	29.87	6.58	10.94	47.39	63.03	13.885	23.085
32	LG 44	49.05	6.78	13.14	68.97	71.118	9.8304	19.052	30.27	6.78	13.14	50.19	60.311	13.509	26.181
Recalculated Value of Q, F, L and Q_m, F, L of Subansiri Formation of Likabali-Garo section															
33	KZ 1(2)	56.2	6.84	10.65	73.69	76.265	9.2821	14.452	51.99	6.84	10.65	69.48	74.827	9.8446	15.328
34	KZ 3	54.17	6.43	12.7	73.3	73.902	8.7722	17.326	52.7	6.43	12.7	71.83	73.368	8.9517	17.681
35	KZ 6	52.255	6.32	9.42	67.995	76.851	9.2948	13.854	50.02	6.32	9.42	65.76	76.064	9.6107	14.325
36	KZ 8	55.28	7.82	10.69	73.79	74.915	10.598	14.487	52.68	7.82	10.69	71.19	73.999	10.985	15.016
Recalculated Value of Q, F, L and Q_m, F, L of Kimin Formation of Kimin-Ziro section															
37	KZ 12	47.44	5.94	14.08	67.46	70.323	8.8052	20.872	29.15	5.94	14.08	49.17	59.284	12.081	28.635
38	KZ 14	49.36	6.02	10.88	66.26	74.494	9.0854	16.42	22.97	6.02	10.88	39.87	57.612	15.099	27.289
Recalculated Value of Q, F, L and Q_m, F, L of Dafla Formation of Kimin-Ziro section															
39	KZ 17	49.77	7.1	12.37	69.24	71.88	10.254	17.865	25.69	7.1	12.37	45.16	56.887	15.722	27.391
40	KZ 22	50.275	6.98	11.34	68.595	73.293	10.176	16.532	30.67	6.98	11.34	48.99	62.605	14.248	23.148
Recalculated Value of Q, F, L and Q_m, F, L of Subansiri Formation of Kimin-Ziro section															

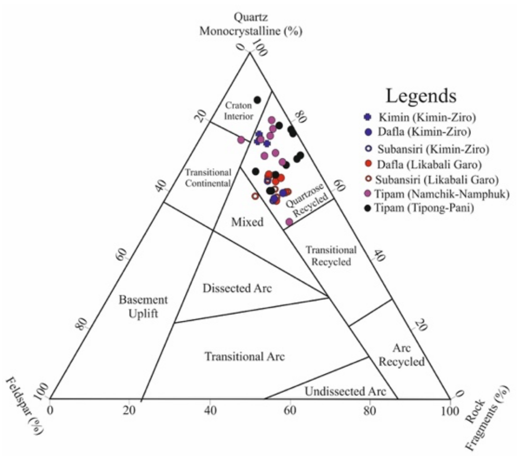

Fig. 6. QmFL tectonic discrimination diagram after Dickinson (1985) illustrating the provenance fields of sandstones from all four sections

within the quartzose recycled provenance field (Fig. 6). Such clustering indicates multicycle sediment derivation from quartz-enriched orogenic sources rather than primary cratonic input. Rare outliers in transitional continental or mixed provenance fields are statistically insignificant and do not alter the dominant tectonic signal.

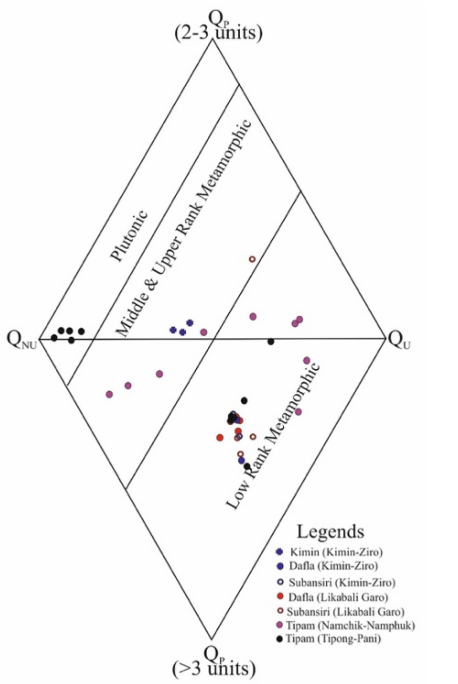

Fig. 7. Diamond provenance diagram after Basu et al. (1975) showing the distribution of quartz types for sandstones from all four sections.

Diamond plots after Basu et al. (1975) (Fig. 7) refine the source characterization. Most samples plot within the low-rank metamorphic field, with subordinate distribution toward the middle- to upper-rank metamorphic and plutonic fields. The clustering pattern indicates dominant sediment derivation from low-grade metamorphic terranes, with localized input from higher-grade metamorphic complexes and granitoid sources, reflecting progressive unroofing of an evolving orogenic hinterland.

Tortosa et al. (1991) (Fig. 8) also refine the source characterization. Most samples plot within the Slates & Schists and Gneisses fields, indicating dominant derivation from low- to medium-grade metamorphic terranes, whereas subordinate samples extend into the Granite and mid- to upper-rank metamorphic fields. The overall distribution pattern reflects sediment supply from a polyphase orogenic hinterland characterized by progressive exhumation of metamorphic complexes and localized granitoid intrusions, consistent with foreland basin sedimentation adjacent to an active continental collision zone. Low-grade metamorphic signatures dominate in the Likabali–Garo section and parts of Tipong–Pani (Fig. 7 and Fig. 8). Middle- to upper-grade metamorphic sources, including gneissic terranes, are more prominent in the Namchik–Namphuk and Kimin–Ziro sections, especially within the Kimin Formation (Fig. 7 and Fig. 8). Granitic fields identified in Tipong–Pani and Kimin–Ziro confirm exposure of plutonic bodies during progressive exhumation. These results collectively indicate derivation from a tectonically active orogenic hinterland characterized by vertical unroofing, differential exhumation, and sustained sediment recycling.

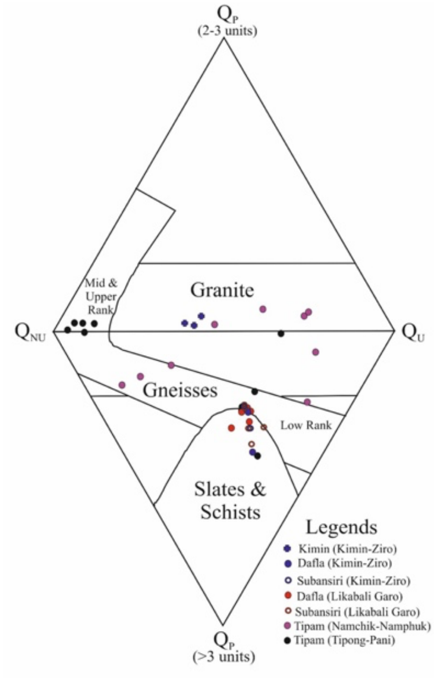

Fig. 8. Diamond provenance diagram after Tortosa et al. (1991) showing the distribution of quartz and inferred source rock fields for sandstones from all four sections.

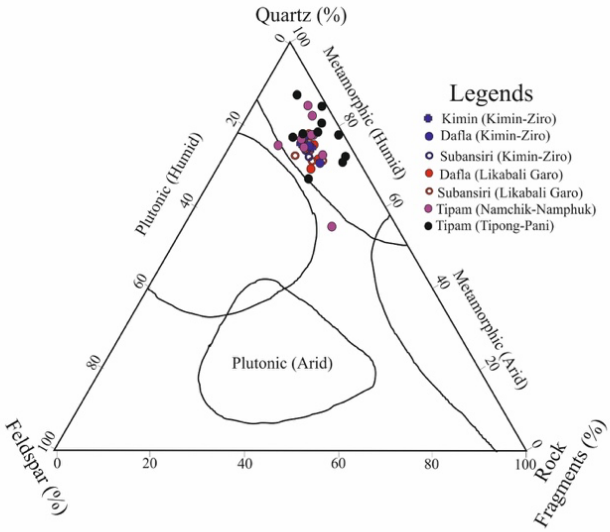

Fig. 9. QFR ternary diagram (Folk, 1980) showing paleoclimatic discrimination fields (humid vs. arid)

PALEOCLIMATE AND WEATHERING REGIME

Compositional paleoclimate proxies consistently indicate sediment generation under humid to semi-humid climatic conditions, amplifying chemical weathering and compositional maturity. In the QFR ternary diagram (Folk, 1980), samples from all four sections cluster within the metamorphic source field, consistent with intense chemical alteration of uplifted basement rocks (Fig. 9). The majority of samples cluster within the metamorphic (humid) field near the quartz apex, indicating derivation under humid to semi-humid climatic conditions that promoted intense chemical weathering and quartz enrichment. Minimal dispersion toward plutonic (arid) domains suggests limited arid-climate influence and reinforces the interpretation of climate-enhanced sediment recycling within an actively uplifting orogenic source region.

In the Qp/(F+RF) versus Qt/(F+RF) binary plot (Basu et al., 1975), most samples plot within the semi-humid to humid fields (Fig. 10), reflecting high quartz proportions relative to feldspar and lithic fragments. This distribution indicates intense chemical weathering and sediment recycling under sustained precipitation, with minimal representation in arid domains, thereby supporting deposition under predominantly humid climatic conditions within an actively uplifting orogenic source region. The Weltje (1994) weathering intensity diagram (Fig. 11) further corroborates moderate to high chemical weathering regimes, with samples clustering predominantly within Fields 1 and 2. These fields correspond to tropical humid to subhumid conditions and are typically associated with low to moderate relief source areas undergoing continuous denudation. The integration of climatic proxies with tectonic indicators suggests that chemical weathering operated synergistically with tectonic uplift to enhance sediment recycling and quartz concentration.

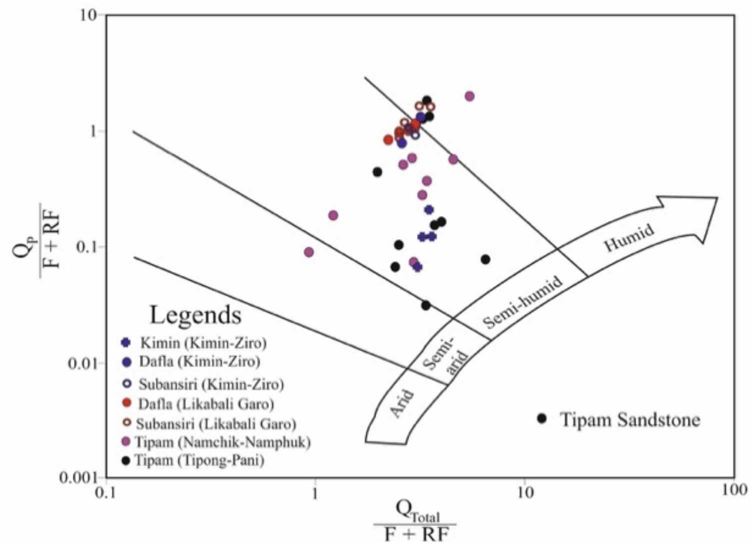

Fig. 10. Binary paleoclimatic discrimination diagram (after Suttner and Dutta, 1986) showing the relationship between Qp/(F+RF) and Qt/(F+RF) ratios for sandstones from all four sections

DEPOSITIONAL ENVIRONMENT

The integrated petrographic, tectonic discrimination, and paleoclimatic evidence indicate deposition within a foreland basin system receiving sediment from an actively uplifting orogenic belt. The dominance of quartzose recycled signatures, coupled with abundant metamorphic lithic fragments and evidence of progressive unroofing, suggests sediment derivation from a fold–thrust hinterland undergoing sustained exhumation. High quartz content and compositional maturity imply prolonged sediment residence time and multicycle reworking, consistent with fluvial transport across broad alluvial plains prior to final deposition. The humid to semi-humid climatic regime inferred from compositional proxies would have enhanced chemical weathering in the source region, promoting feldspar breakdown and quartz enrichment before basin accumulation. Together, these characteristics are consistent with deposition in a fluvio-deltaic to shallow marginal foreland basin setting, where high sediment flux from an evolving collision zone was redistributed through channelized systems and periodically reworked during basin subsidence and accommodation development.

INTEGRATED TECTONIC SYNTHESIS

When integrated regionally, the petrographic, tectonic discrimination, and paleoclimatic datasets converge on a single robust interpretation. The Neogene sandstones of the Namchik–Namphuk, Tipong–Pani, Likabali–Garo, and Kimin–Ziro sections were derived from an actively uplifting recycled orogenic belt characterized by exposure of low- to high-grade metamorphic rocks and granitoid intrusions. The dominance of quartzose recycled signatures in both QFL and QmFLt space unequivocally indicates sediment derivation from a fold–thrust belt undergoing progressive exhumation rather than from stable cratonic interiors.

Spatial variations in quartz types and metamorphic rank reflect differential unroofing levels within the hinterland, documenting vertical tectonic evolution during basin development. The consistent paleoclimatic signal of humid to semi-humid conditions further implies that chemical weathering intensified quartz enrichment and facilitated multicycle sediment recycling.

Overall, the data strongly support deposition within a tectonically active foreland basin system adjacent to a continental collision zone. Sediment supply was governed by sustained orogenic uplift, progressive basement exhumation, and climate-enhanced chemical weathering, producing quartz-rich, compositionally mature sandstones that record the dynamic coupling of tectonics and surface processes during Neogene basin evolution.

COMPARATIVE ANALYSIS

The Neogene period witnessed a very significant episode of the geological evolution of northeastern India, which was essentially driven by the convergence of the Indian and Eurasian plates. Comparative analysis of Neogene rock formations in two tectonically active regions: the Siwalik fold-thrust belt in Arunachal Pradesh and the Belt of Schuppen in the Naga-Patkai Hills of Upper Assam, shows a lot of similarity in sedimentological characteristics, tectonic frameworks, climatic conditions

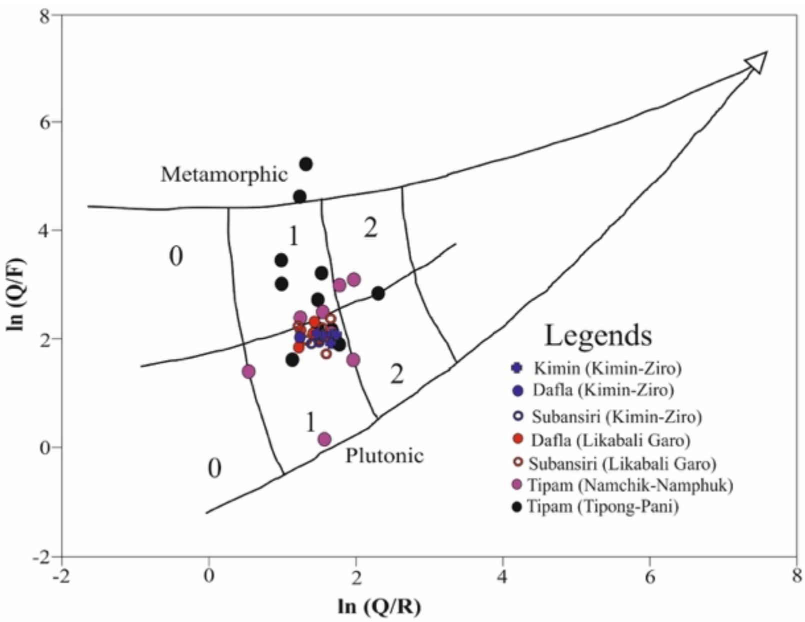

Fig. 11. Weltje (1994) weathering intensity diagram showing the relationship between lnQ/F and lnQ/R ratios for sandstones from all four sections and depositional environments (Bharali and Borgohain, 2013).

In the Belt of Schuppen, Naga-Patkai Hills, Tipam Sandstone from the Namchik-Namphuk and Tipong-Pani sections have Quartz as the most dominant mineral. In the Tipong-Pani section, there exists a significant variation in Quartz content within Tipam sandstone, Girujan sandstone and Dihing sandstone. This can be attributed to the maturity of the sediments as well as tectonic compaction. In the case of Tipam Sandstone, metamorphic rock fragments contribute the most to the rock fragments. At the same time, Girujan Sandstone and Dihing Sandstone report higher abundances of sedimentary rock fragments than metamorphic and igneous rock fragments. However, there is a gradual increase in the amount of metamorphic rock fragments. This is because of the sediments derived from the Naga-Patkai Hills, as well as from the nearby Mishmi Hills. A sporadic increase in the metamorphic rock fragments can be attributed to a faster rate of uplift of the Mishmi Hills. In contrast, a faster rate of upliftment of the Naga-Patkai Hills resulted in a higher contribution of igneous and sedimentary rock fragments in the Tipam Group of rocks. The high percentage of quartz and the mature shapes of the grains indicate that the sediments are recycled orogeny sediments. The rocks are formed in a temperate subhumid and tropical humid climatic condition with moderate to low relief for sedimentation.

Quartz is the most dominant mineral in the rocks of the Siwalik Belt as well. Rocks from the Kimin-Ziro and Likabali-Garo sections reveal variations in quartz content within the Dafla, Subansiri and Kimin Formations. This variation can be explained in terms of varying degrees of tectonic compaction and sedimentary maturity. They contain a higher amount of metamorphic rock fragments than igneous and sedimentary rock fragments. The distribution of rock fragments can be interpreted with the help of the changing rate of uplift of the Himalaya. Faster uplifting of the Higher Himalaya led to metamorphism, contributing metamorphic rock fragments to the sediments. Occasional increase in fragments of igneous rocks suggests some influence from the Lesser Himalayas.

Table 6: Distribution of rock fragments

Sample name	Sl. No.	Rock fragments				Recalculation of Rock fragments in %		
		Igneous	Sedimentary	Metamorphic	Total	Igneous	Sedimentary	Metamorphic
NR1	1	3.52	1.49	5.64	10.65	33.05	13.99	52.96
NR2	2	3.16	2.07	4.97	10.2	30.98	20.29	48.73
NR3	3	2.53	0.81	2.78	6.22	40.68	13.02	44.69
NR4	4	2.871	11.89	7.469	22.23	12.91	53.49	33.60
NR5	5	0.924	1.91	8.006	10.84	8.52	17.62	73.86
NR6	6	1.003	6.73	0.664	7.73	12.98	87.06	8.59
NR7	7	0.86	1.29	6.63	8.86	9.71	14.56	74.83
NR8	8	2.97	4.06	9.54	15.66	18.97	25.93	60.92
NR9	9	2.096	1.004	8.4	11.5	18.23	8.73	73.04
Results of Tipam Sandstone Formation of Namchik river section								
4(C)	10	3.14	1.82	7.12	11.08	28.34	16.43	64.26
2(I)	11	1.28	13.44	5.06	19.32	6.63	69.57	26.19
2(D)	12	1.975	9.43	3.98	15.63	12.64	60.33	25.46
2(H)	13	1.62	13.065	3.05	17.4	9.31	75.09	17.53
P(3)	14	0.53	6.1	1.43	7.53	7.04	81.01	18.99
P(4)	15	4.04	10.05	2.65	14.74	27.41	68.18	17.98
P(5)	16	4.002	14.6	1.9	19.5	20.52	74.87	9.74
P(6)	17	2.5	4.425	2.091	8.94	27.96	49.50	23.39
P(7)	18	1.097	8.438	2.005	11.54	9.51	73.12	17.37
P(8)	19	0.095	6.9	3.95	11.94	0.80	57.79	33.08
P(9)	20	1.66	6.47	2.21	10.34	16.05	62.57	21.37
Results of Tipam Sandstone Formation of Tipong Pani river section								
LG 4(2)	21	0.65	1.25	8.1	10	6.50	12.50	81.00
LG 9(3)	22	2.35	2	9.13	13.48	17.43	14.84	67.73
LG 10 (1)	23	1.07	1.13	12.08	14.28	7.49	7.91	84.59
LG 13	24	1.56	0.86	8.36	10.78	14.47	7.98	77.55
LG 19 (2)	25	1.01	3.87	7.21	12.09	8.35	32.01	59.64
LG 21 (3)	26	0.73	1.65	9.5	11.88	6.14	13.89	79.97
LG 23	27	1.2	1.77	7.4	10.37	11.57	17.07	71.36
LG 25	28	2.07	3.22	9.08	14.37	14.41	22.41	63.19
LG 31	29	2.22	1.8	5.82	9.84	22.56	18.29	59.15
LG 35	30	3.74	3.38	3.75	10.87	34.41	31.09	34.50
LG 39 (2)	31	2.305	2.385	6.25	10.94	21.07	21.80	57.13
LG 44	32	1.1	1.015	11.025	13.14	8.37	7.72	83.90
Result of Siwalik Group of Likabali-Garo section								
KZ 1(2)	33	2.1	0.45	8.1	10.65	19.72	4.23	76.06
KZ 3	34	2.03	2.05	8.62	12.7	15.98	16.14	67.87
KZ 6	35	1.59	0.9	6.93	9.42	16.88	9.55	73.57
KZ 8	36	0.599	0.591	9.5	10.69	5.60	5.53	88.87
KZ 12	37	4.1	3.09	6.89	14.08	29.12	21.95	48.93
KZ 14	38	1.33	1	8.55	10.88	12.22	9.19	78.58
KZ 17	39	10.07	0.4	1.9	12.37	81.41	3.23	15.36
KZ 22	40	1.1	0.6	9.64	11.34	9.70	5.29	85.01
Result of Siwalik Group of Kimin- Ziro Road section								

Modal analysis reveals that the sediments are of recycled orogeny. The climatic condition of deposition of Neogene rocks of the Siwalik Belt is similar to the Naga Schuppen Belt, i.e., temperate subhumid and tropical humid climatic conditions with moderate to low relief for sedimentation.

ROCK FRAGMENT ANALYSIS

For proper analysis of the rock Fragments, individual rock fragments present in each petrographic thin section are identified, and their numbers are counted. Considering their total as 100%, each type of rock fragments is normalized and recalculated (Table 6). The study of rock fragments reveals certain characteristic details of the broader regional geology of this region. The result of rock fragment analysis is quite synchronous with the established regional geology of the region. In fact, these rock fragments can be used to interpret the provenance of the sediments (Boggs, 2013).

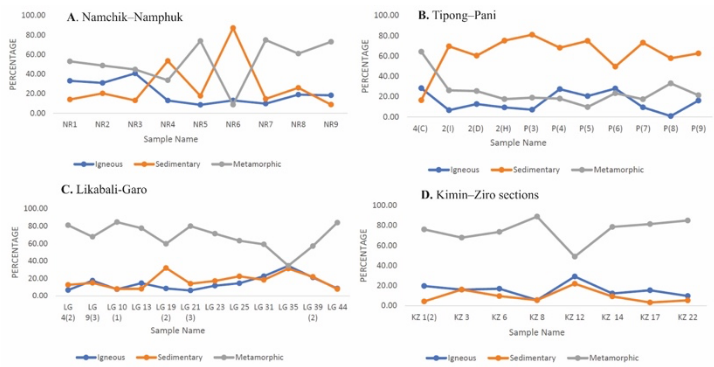

Fig. 12. Bivariate plot showing the distribution of Rock-fragments: A. Namchik–Namphuk, B. Tipong–Pani, C. Likabali-Garo and D. Kimin–Ziro sections

Table 6 reveals that the Tipam Sandstone of the Namchik-Namphuk section is rich in metamorphic rock fragments, with a notable presence of igneous fragments as well (Fig. 12). This composition aligns with the regional geology, where the Mishmi Hills emerge as the primary contributor to sediment supply. The Mishmi massif is characterized by diverse metamorphic rocks such as gneiss, biotite gneiss, calc-gneiss, garnetiferous gneiss and staurolite-bearing schist, alongside igneous rocks including diorite, granodiorite, quartz diorite, amphibolite, and peridotite (Salvi et al., 2020). Petrographic analysis of rock fragments confirms the presence of these lithologies within the sandstone. Thus, it can be interpreted that the provenance of the Tipam Sandstone in the Namchik-Namphuk section lies within the Mishmi Hills.

At the same time, the Tipam Sandstone of the Tipong-Pani section contains mostly sedimentary rock fragments. The rocks of the Tipong-Pani section are highly influenced by the Naga Patkai ranges. During sedimentation of Tipam Sandstone, Disang and Barail were already uplifted, thereby being vulnerable to sedimentary processes like erosion, transportation and sedimentation. Disang and Barail contributed heavily to the formation of Tipam Sandstone, which can be interpreted by rock fragment studies.

The rocks of Likabali-Garo and Kimin-Ziro sections depict a different picture (Fig. 12). The Siwalik rocks of these two sections are rich in metamorphic rock fragments with minor contributions from igneous and sedimentary rocks. The constituent sediments of the Siwalik Group of rocks were supplied by the Higher Himalaya and Lesser Himalaya. Higher Himalaya contains metamorphic rocks like Schist and Gneiss and igneous rocks like granites, while Lesser Himalaya comprises of metamorphic rocks like Quartzite, Marble, Slate, Phyllite, Schist and Gneiss and minor Volcanic and Granitic rocks. Therefore, the contribution of a higher percentage of metamorphic rocks supports their provenance from the Higher Himalaya and Lesser Himalaya.

EVOLUTION MODEL

The evolution model proposed in this study integrates existing structural and tectonic frameworks developed by earlier workers like Goswami et al. (2021), Salvi et al. (2020) and Yin et al. (2004) with new sedimentological and petrographic data derived from the present investigation. Our findings aim to support rather than redefine them.

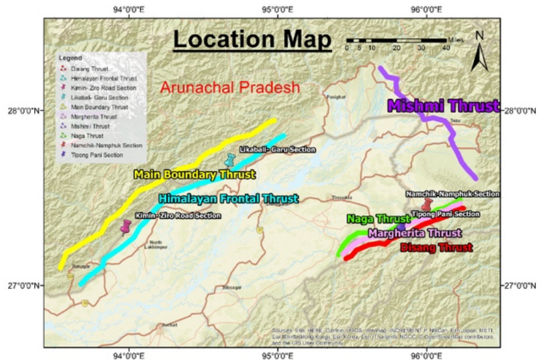

Fig. 13A. Structural Map of study locations

Fig. 13A illustrates the tectonic setting of the four studied sections along Namchik-Namphuk, Tipong-Pani,

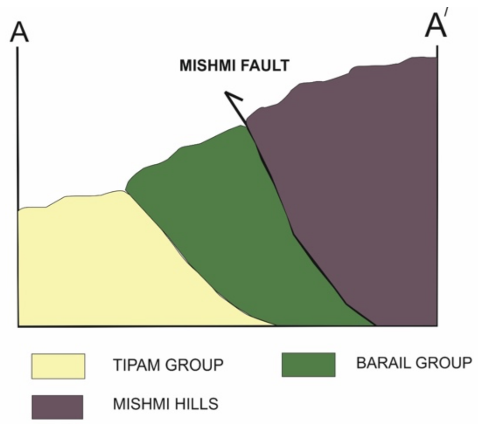

Fig. 13B. Schematic diagram showing formation of Miocene Tipam basin frontal basin of Mishimi hills.

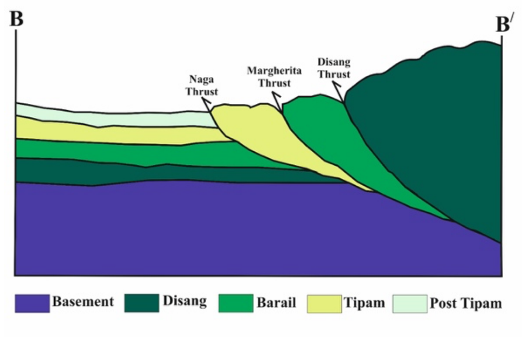

Fig. 13C. Schematic diagram showing formation of Miocene Tipam basin frontal part of Naga Hills

Kimin-Ziro and Likabali-Garo sections within the Himalayan foreland basin system. These sites are positioned within the Himalayan foreland basin, lying in front of the Naga foredeep and the foredeep itself has formed in front of the Mishmi Hills, which emerged due to interactions among three key tectonic elements in the region. During the Miocene period, sediment deposition and uplift processes led to the exposure of various tectonic rock types in these areas (Goswami et al., 2021).

In the Namchik-Namphuk section, dominance of metamorphic and igneous rock fragments over fewer fragments of sedimentary rocks is observed in the Tipam Sandstone (see Fig. 12A). This dominance is attributed to its close proximity to the Mishmi Hills and the Naga Orogeny. During the deposition of the Tipam sediments, the sediment supply primarily originated from both the

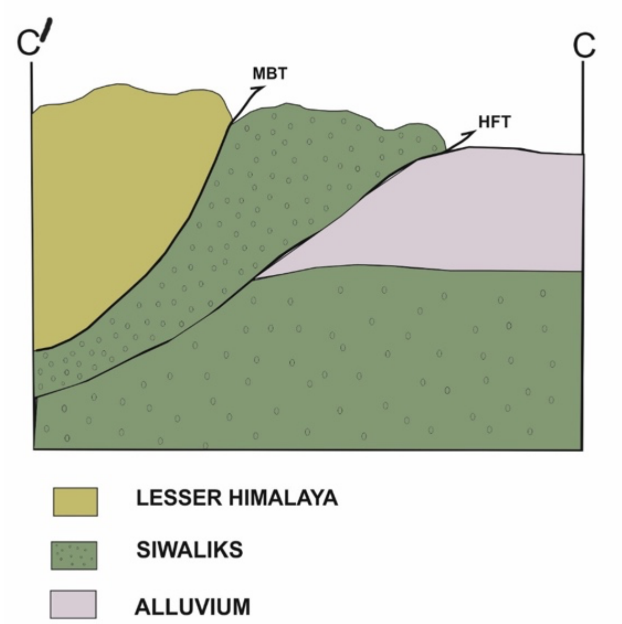

Fig. 13D. Schematic Diagram illustrating the development of the Mio-Pliocene Siwalik basin in frontal part of Sub-Himalaya

Mishmi Hills and the Naga Hills (Fig. 137B) (Salvi et al., 2020).

In the Tipong-Pani section, sedimentary rock fragments are dominant with relatively fewer igneous and metamorphic rock fragments (Fig. 12B). This distribution can be explained in terms of its proximity to the uplifted Naga Hills and the exposed Barail and Disang formations. It corroborates the idea that these older sedimentary sequences were a primary source of deposition of Tipam sediments (Sarma and Chutia, 2013). This spatial relationship is schematically represented in Fig. 13C.

In the Siwalik Belt sections of Kimin-Ziro and Likabali-Garo, predominance of metamorphic rock fragments is observed with minor contribution of igneous and sedimentary source (Fig. 12C and 12D). This sediment was deposited in the Himalayan foredeep in front of the Lesser Himalaya, where the Gondwana Group of rocks is exposed in a narrow strip near the Main Boundary Thrust (MBT) and Himalayan Frontal Thrust (HFT). The Gondwana group in the Lesser Himalaya consists mainly of metamorphic rocks from the Paleogene age. These rocks are intruded by igneous and sedimentary rocks at a few locations. As a result, metamorphic rock fragments are the most abundant in this section, with smaller amounts of sedimentary and igneous rock fragments (Fig. 13D) (Dikshit and Dikshit, 2014; Yin et al., 2004).

Fig. 14 summarizes the inferred tectono-sedimentary evolution of the region during the Miocene-

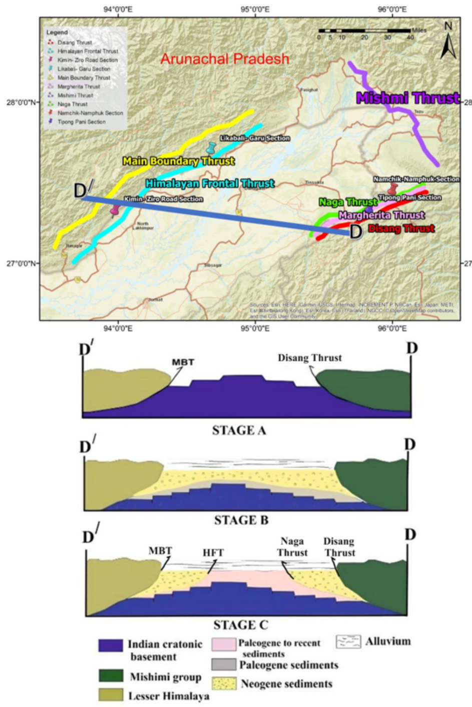

Fig. 14. Schematic Diagram illustrating the development of the Neogene period Upper assam basin

Pliocene. The sediments were deposited in the foredeep developed in front of the Naga orogeny and Himalaya orogeny at stage A. Because of the close proximity of these two orogenies during Miocene time, the foredeep merged from a basin that extended right from the Naga orogeny to the Himalayan orogeny. The resulting sedimentation shaped the upper Assam Basin's structure during the Miocene to Pliocene epochs. Tectonic activity led to the uplift of the Main Boundary Thrust (MBT) in the north and the Naga Thrust in the south, facilitating the development of the frontal basin. The uplift created conditions for Neogene sediment deposition in the foredeep basin on both sides of the Naga-Mishmi Hills and the Himalayas, shaping the region's geological structure and sedimentary evolution as represented in stage B. Due to further thrust displacement, the previously deposited sediments have been restructured, with the Siwalik group uplifted to the north and the Tipam Group uplifted to the south. This tectonic activity led to the formation of a foredeep basin at stage C, where sedimentation has continued from the Paleogene sediments to the present. The ongoing deposition in this basin reflects the dynamic tectonic environment and the persistence of sediment influx over time (Bezbaruah and Goswami, 2013; Borgohain et al., 2023; Singh et al., 2013).

Although the schematic diagrams (Figs. 13 and 14) are conceptual and based primarily on available literature, the petrographic evidence substantiates them. Therefore, this evolution model is not a novel tectonic reconstruction, but a validation and refinement of existing models using new sedimentological datasets.

DISCUSSION

The petrographic, compositional, and provenance data from Neogene sandstones of the Siwalik and Schuppen belts reveal a comprehensive picture of sediment dispersal, basin dynamics, and tectonic influence in the eastern Himalayan foreland system. The Namchik-Namphuk section in the Schuppen Belt is notably enriched in polycrystalline and undulatory monocrystalline quartz, kink-banded muscovite, and metamorphic rock fragments, which collectively indicate a dominant contribution from medium- to high-grade metamorphic terranes of the Mishmi Hills. These lithologies, characterized by gneissic, schistose, and granodioritic signatures, suggest rapid erosion and proximal deposition along the Mishmi Thrust front during an active phase of orogenic uplift in the Neogene. In contrast, the Tipong-Pani section reflects a sedimentary dominance, where lithic fragments are predominantly derived from uplifted and eroded older sequences such as the Barail and Disang Groups. The petrographic maturity of Tipam sandstones here, along with the abundance of non-undulatory quartz and laminated sedimentary fragments, points to a recycled origin from pre-existing foreland successions under lower-energy fluvial or deltaic conditions. This variation between Namchik-Namphuk and Tipong-Pani sections highlights lateral facies differentiation controlled by spatial proximity to distinct tectonic source zones-Mishmi versus Naga Hills. In the Siwalik Belt, the Kimin-Ziro and Likabali-Garo sections present high proportions of quartz, moderate feldspar, and abundant metamorphic lithics, indicating consistent sediment input from the Higher and Lesser Himalayas. Textural characteristics such as overgrowth on quartz grains, twinning in microcline and plagioclase, and low matrix content suggest relatively rapid sediment delivery under tectonically induced high-relief conditions. Modal data plotted in QFL and QmFLt ternary diagrams clearly cluster within the recycled orogenic provenance fields, reinforcing the interpretation of sediment sourcing from uplifted metamorphic and granitic terrains undergoing multicyclic erosion and reworking (Goswami et al., 2020). Climatic influences, inferred from QFR and Weltje diagrams, show that deposition in all sections occurred under tropical humid to subhumid conditions, enhancing chemical weathering, particularly of feldspar, and promoting clay-rich matrix development in more distal zones such as Tipong-Pani and Likabali-Garo. The sediment composition, therefore, is a product of both tectonically driven uplift and climate-controlled weathering, with intense monsoonal regimes accelerating feldspar alteration and sediment recycling. The evolution of these foreland systems was further shaped by flexural subsidence and thrust loading associated with the Indian-Eurasian and Indian-Burma plate convergence. In this tectonic context, the merging of the Himalayan foredeep with the Naga-Mishmi foreland basin during the Miocene–Pliocene allowed for integrated sediment routing systems across the Brahmaputra arc. Variability in the types and proportions of lithic fragments, metamorphic in Namchik-Namphuk and Siwalik sections, sedimentary in Tipong-Pani, also reflects diachronous uplift phases, differential erosion rates, and catchment area evolution. These contrasts underscore a dynamic interplay of sediment supply, depositional energy, and basin architecture. The Schuppen Belt reflects more distal, recycled sedimentation, influenced by reworking of older orogen-derived units, while the Siwalik Belt records more proximal, first-cycle deposits from active Himalayan thrust sheets. Together, these findings portray the Neogene foreland basins of Northeast India as evolving sedimentary systems shaped by both spatial and temporal variability in tectonic uplift, erosion intensity, climatic regimes, and structural accommodation space, offering a nuanced understanding of sedimentary processes in an orogen-foreland setting.

CONCLUSIONS

This study provides a comprehensive sedimentological and petrographic assessment of Neogene sandstones from two tectonically distinct foreland basins in Northeast India-the Siwalik Belt of Arunachal Pradesh and the Belt of Schuppen in the Naga-Patkai Hills. By analyzing the modal composition, quartz types, feldspar and mica textures, and lithic fragment assemblages, the research effectively distinguishes the sedimentary imprints of two different orogenic systems: the Himalayan thrust front and the Mishmi-Naga domain. The Namchik-Namphuk section reveals a clear metamorphic and igneous provenance linked to the Mishmi Hills, while the Tipong-Pani section reflects recycled sedimentary sources from uplifted Disang and Barail formations. In contrast, the Siwalik sections- Likabali-Garo and Kimin-Ziro-are characterized by high quartz content, feldspar variability, and metamorphic rock fragments indicative of sediment supply from the Higher and Lesser Himalayas.

A notable contribution of this work is the application of rock fragment analysis as a diagnostic tool for provenance differentiation, allowing a nuanced understanding of tectonic inputs and basin evolution. The study demonstrates how variations in sediment composition correspond to shifts in depositional energy, proximity to thrust fronts, and the intensity of chemical weathering, influenced by both climate and tectonics. It also illustrates how the convergence-driven uplift of multiple orogenic systems facilitated distinct sediment dispersal patterns, which eventually merged across the Brahmaputra arc during the Miocene–Pliocene.

By establishing a clear lithological and tectonic contrast between the Naga Schuppen and Siwalik belts, the study enhances current models of foreland basin dynamics and sediment routing in complex collisional settings. It contributes original field-based evidence that supports broader theories of sediment recycling and tectonic reactivation, reinforcing the role of rock fragments as reliable proxies for reconstructing past geodynamic environments. Overall, the findings deepen the geological understanding of sediment generation and transport in a region critical to the tectonic evolution of the eastern Himalaya and adjoining Indo-Burman ranges.

ACKNOWLEDGEMENT

The authors express their deepest gratitude to the Oil India Limited-sponsored KDM Chair of the Department of Applied Geology, Dibrugarh University, for providing financial support and resources essential for the successful completion of this research. Special thanks are extended to Dr. Devojit Bezbaruah for his invaluable guidance, insights, and encouragement throughout the study. His expertise and mentorship have greatly contributed to the quality and depth of this work. The authors also acknowledge the support of faculty, colleagues, and all those who assisted directly or indirectly in this research endeavor.

AUTHOR'S CONTRIBUTION

Abhijit Chakraborty contributed to all aspects of the study, including fieldwork, data analysis, Figures, review, and manuscript preparation. Monmohan Gogoi assisted in manuscript writing, figure preparation and editing. Persona Gogoi prepared all the illustrations. Ranjan Kumar Sarmah guided the field planning and logistics. Diganta Bhuyan supported manuscript structuring and review. All authors reviewed and approved the final version.

FUNDING

This research was financially supported by the Oil India Limited-sponsored K.D.M. Chair, Department of Applied Geology, Dibrugarh University.

DECLARATION OF CONFLICTING INTERESTS

The authors declare that they have no known competing interests or personal relationships that could have appeared to influence the work reported in this paper.

REFERENCES

Basu, A., Young, S. W., Suttner, L. J. (1975). Re-evaluation of the use of undulatory extinction and polycrystallinity in detrital quartz for provenance interpretation; Journal of Sedimentary Petrology, v. 45(4), p. 873–882.

Bezbaruah, D. and Goswami, T. K. (2013), Siwalik foreland fold and thrust belt along Gai River section, Arunachal Pradesh: A field guide; South East Asian Journal of Sedimentary Basin Research, v. 1(2), p. 86–95.

Bharali, B. and Borgohain, P. (2013), Few characteristics of Tipam Sandstone Formation within oilfield areas of Upper Assam: A study based on wireline log data; Journal of Earth Science, Special Volume, p. 36–45.

Boggs, S. Jr. (2013). Principles of Sedimentology and Stratigraphy; Pearson Education.

Borgohain, P., Pandey, N., Sangeeta, A., Khalo, A. (2023), Depositional environment and provenance of Tipam Sandstone Formation exposed in parts of Naga Schuppen Belt, Naga Hills, NE India; Science Vision, v. 23(4), p. 66–71.

Carver, R. E. (1971). Procedures in Sedimentary Petrology; Wiley-Interscience.

Catlos, E. J., Dubey, C. S., Harrison, M. T., Edwards, M. A. (2004), Late Miocene movement within the Himalayan Main Central Thrust shear zone, Sikkim, North-East India; Metamorphic Evolution of the Sikkim Himalayas, India, p. 207–226.

Dickinson, W. R. (1985). Interpreting provenance relations from detrital modes of sandstones; Provenance of Arenites, NATO ASI Series C, v. 148, p. 333–363.

Dickinson, W. R., Beard, L. S., Brakenridge, G. R., Erjavec, J. L., Ferguson, R. C., Inman, K. F., Ryberg, P. T. (1983), Provenance of North American Phanerozoic sandstones in relation to tectonic setting; Geological Society of America Bulletin, v. 94(2), p. 222–235.

Dikshit, K. and Dikshit, J. (2014), Structural framework; North-East India: Land, People and Economy, p. 61–90.

Folk, R. L. (1980). Petrology of Sedimentary Rocks; Hemphill Publishing Company.

Goswami, T. K., Bezbaruah, D., Mahanta, B. N., Sarmah, R. K. (2021), Structural framework, crustal shortening and Cenozoic exhumation in the Eastern Himalaya: A review; Physics and Chemistry of the Earth, v. 124(2), p. 1–25.

Goswami, T. K., Mahanta, B. N., Mukherjee, S. (2020). Orogen-transverse structures in the Eastern Himalaya: Dextral Riedel shear along the Main Boundary Thrust in the Garo-Gensi area (Arunachal Pradesh, India), implication in hydrocarbon geoscience; Marine and Petroleum Geology, v. 114, p. 1–17.

Grantham, J. H. and Velbel, M. A. (1988), The influence of climate and topography on rock fragment abundance in modern fluvial sands of the Southern Blue Ridge

Mountain, North Carolina; Journal of Sedimentary Petrology, v. 58(2), p. 219–227.

GSI, (2010). Geology and Mineral Resources of Arunachal Pradesh, vol. 30 GSI, Misc Pub IV, I.

Krumbein, W. C. and Pettijohn, F. J. (1938), A Manual of Sedimentary Petrography; Appleton-Century-Crofts.

Kumar, G. (1997). Geology of Arunachal Pradesh, Geol. Soc. Ind, Bangalore, 217p.

Salvi, D., Mathew, G., Kohn, B., Pande, K., Borgohain, B. (2020), Thermochronological insights into the thermotectonic evolution of Mishmi Hills across the Dibang Valley, NE Himalayan Syntaxis; Journal of Asian Earth Sciences, v. 190, p. 1–19.

Sarma, J. N. and Chutia, A. (2013), A comparative sedimentological study of Tipam Sandstone Formation exposed along Tipong-Pani and Dilli Ghat sections, Upper Assam, India; Journal of Earth Science, Special Volume, p. 72–80.

Singh, A. K., Singh, M. P., Singh, P. K. (2013). Petrological investigations of Oligocene coals from foreland basin of Northeast India; Energy Exploration and Exploitation, v. 31, p. 909–936.

Suttner, L.J. and Dutta, P.K. (1986), Alluvial Sandstone Composition and Paleoclimate, Framework Mineralogy; Journal of Sedimentary Petrology, 56, p. 329-345.

Tortosa, A., Palomares, M., Arribas, J. (1991). Quartz grain types in Holocene deposits from the Spanish Central System: Some problems in provenance analysis; Developments in Sedimentary Provenance Studies, Geological Society of London, Special Publication, v. 57, p. 47–54.

Weltje, G. J. (1994). Provenance and Dispersal of Sand-sized Sediments; Sedimentary Geology Series.

Yin, A., Kelty, T. K., Dubey, C., Gehrels, G., Chou, Q., Grove, M., Lovera, O. (2004), Structural framework of the westernmost Arunachal Himalaya, NE India; Himalayan Journal of Sciences, v. 2(4-Special Issue), p. 284.